NUCL SCI TECH (2019) 30:14
https://doi.org/10.1007/s41365-018-0536-4

Nuclear collectivity in the even–even $^{164-178}$Yb along the yrast line

Hui-Fang Li[1] · **Hua-Lei Wang**[1] · **Min-Liang Liu**[2]

Received: 5 June 2018 / Revised: 18 September 2018 / Accepted: 19 September 2018 / Published online: 2 January 2019

Abstract The collective properties along the yrast line in well-deformed even–even $^{164-178}$ Yb isotopes are investigated by pairing self-consistent total Routhian surface (TRS) calculations and extended E-gamma over spin (E-GOS) curves. The calculated results from ground-state deformations, e.g., β_2, are in agreement with previous theoretical predictions and available experimental data. The basic behaviors of moment of inertia are reproduced by the present TRS calculations and discussed based on the aligned angular momenta. The centipede-like E-GOS curves indicate that the non-rotational components appear along the yrast sequences in these nuclei, which can explain the discrepancy in the moment of inertia between theory and experiment to some extent. The further extended E-GOS curves, which include the first-order rotation–vibration coupling, appear to provide possible evidence of vibrational effects in the well-deformed nuclei of $^{164-178}$Yb.

This work was supported by the National Natural Science Foundation of China (No. 11675148), the Project of Youth Backbone Teachers of Colleges and Universities of Henan Province (No. 2017GGJS008), the Outstanding Young Talent Research Fund of Zhengzhou University (No. 1521317002), and the Physics Research and Development Program of Zhengzhou University.

✉ Hua-Lei Wang
wanghualei@zzu.edu.cn

1 School of Physics and Engineering, Zhengzhou University, Zhengzhou 450001, China

2 Institute of Modern Physics, Chinese Academy of Sciences, Lanzhou 730000, China

Keywords Vibrational effect · Total Routhian surface calculation · E-GOS curve

1 Introduction

Thanks to the development of experimental techniques such as highly effective γ-ray detector arrays and radioactive beam facilities, nuclear physicists are increasingly interested in the study of nuclear shapes, in particular at extreme conditions of excitation energy or spin or isospin of nuclei. Indeed, the model of spherical nuclei cannot completely reflect the reality of nuclear structure because very few nuclei, in the entire nuclear chart, have this shape even in their ground states. The spherical shapes prevail only near closed shells, while between closed shells the large number of valence nucleons in orbits with large single-particle angular momentum may lead to large deformations of nuclei. Typically, deformed nuclei can be schematically subdivided into prolate, oblate, and triaxial nuclei according to the three principal axes of rotation in the ellipsoid. Meanwhile, experiments and/or theories have revealed some exotic shapes [1]. It is known that many nuclei in the rare-earth area are well deformed (e.g., with quadrupole deformation $\beta_2 > 0.2$) at ground or low-lying states [2]. The well-deformed nuclei often exhibit collective rotational properties with the energy spectrum approximating the typical relation of $E \propto I(I+1)$. Because nuclear rotation can also change its microscopic structure, the preferred shapes of nuclei usually change with increasing spin, especially for the soft nuclei. Certainly, many nuclei show a mixed character with both vibrational and rotational features. During the past several decades, numerous studies have been conducted using various theoretical approaches, including semi-empirical methods, mean-field models, beyond mean-field models (e.g., particle-rotor model [3–5], cranked shell model [6–8], projected shell model [9], cranking covariant density functional theory [10], etc.). However, none of them alone can fully describe the data, mainly due to certain scarce effects in the theoretical modeling. Such empirical methods are often useful for testing the possible missing mechanisms.

Regan et al. have suggested a simple method, namely the E-gamma over spin (E-GOS), which can be used to discern the shape and phase evolution between vibrational and rotational modes in nuclei as a function of spin [11]. In our previous work, we further developed the E-GOS curve to a centipede-like E-GOS one, and simultaneously included the γ-soft motion mode [12–14]. In this work, taking the well-deformed nuclei $^{164-178}$Yb as examples, we would like to investigate their rotational properties along the yrast line by using the pairing-deformation self-consistent TRS method [6, 7, 12, 15] without including the vibrational effect. Namely, pairing is treated self-consistently at each frequency and each grid point in the selected deformation space, and the equilibrium deformations are determined by minimizing the calculated TRS. Close attention is paid to the difference between theoretical calculations and experimental data. Considering the first-order vibrational-rotational coupling effect, this work presents an empirically extended E-GOS curve that may provide evidence of vibrational effects in these well-deformed nuclei. This method could also be easily extended to other nuclear regions and odd-A nuclei.

The article is organized as follows. In Sect. 2, we present a brief description of the theoretical method. Section 3 is devoted to the numerical calculation results and discussions. Finally, a brief summary is given in Sect. 4.

2 Theoretical descriptions

The present TRS calculation method is based on the macroscopic–microscopic model and the cranked shell model (CSM) [6, 7] which usually well accounts for the high-spin properties in rapidly rotating medium and heavy mass nuclei [16–18]. The total energy in a rotating frame of reference, namely the "total Routhian," is the sum energy of the non-rotating state and the contribution due to cranking. The static energy consists of a macroscopic part usually expressed by the standard liquid-drop model [19], and a microscopic term which can be evaluated from a set of Woods–Saxon single-particle levels [14, 16] by using the well-known Strutinsky method [20]. Such a shell-correction method can optimize the liquid-drop energy and give relatively high accuracy, which is usually superior to that of the microscopic models based on effective nucleon–nucleon interactions. It should be noted that we treat the pairing correlation using the Lipkin–Nogami (LN) approach [21], in which the particle number is approximately conserved. In that case, the spurious pairing phase transition encountered in the usual BCS calculation can be avoided. In this work, both monopole and doubly stretched quadrupole pairings are considered, and their strengths are determined using the average gap method [22] and restoring the Galilean invariance broken by the seniority pairing force [7, 23], respectively. Under rotation, a nuclear system is constrained to rotate around a fixed axis (e.g., the x-axis) at a given frequency. That is, the energy contribution from cranking can be obtained by solving the cranking LN equations, which have similar forms to the well-known Hartree–Fock–Bogolyubov cranking (HFBC) equations [7]. We perform the present calculation in the $(\beta_2, \gamma, \beta_4)$ deformation space and only consider the one-dimensional cranking around the principal axis that possesses the largest moment of inertia. Such calculation is valid for most nuclei, especially for the well-deformed ones. Additional theoretical descriptions can be found in Refs. [14, 24] and references therein. The empirical E-GOS [E-gamma over spin, namely the function $R(I) = E_\gamma(I \rightarrow I-2)/I$] curve was first proposed to manifest the shape/phase transition between vibration and rotation along the yrast line [11]. For a perfect harmonic vibrator, a γ-soft rotor, and an axially symmetric rotor, it is easy to derive that the function relationships between $R(I)$ and I will be $E_\gamma(2 \rightarrow 0)/I$, $E_\gamma(2 \rightarrow 0)[1/4 + 1/(2I)]$, and $E_\gamma(2 \rightarrow 0)[2/3 - 1/(3I)]$, respectively. Based on this idea, we developed the centipede-like E-GOS curve in Refs. [12, 13], where the effective factor $E_\gamma^{\mathrm{eff.}}(2 \rightarrow 0)$ was used. In this work, we will further improve the E-GOS curve by including in the energy formula the first-order rotation–vibration coupling [25],

$$E(I) = aI(I+1) + b[I(I+1)]^2, \tag{1}$$

where a and b are constants. After a simple derivation, the $R(I)$ in this situation will be

$$R(I) = f(I)(2 - 1/I), \tag{2}$$

where the spin-dependent factor $f(I)$ is

$$f(I) = 2a + 2b[I(I+1) + (I-2)(I-1)]. \tag{3}$$

Of course, one can easily obtain the constants a and b from two arbitrarily selected and adjacent energy levels $E^{\mathrm{s}}(I^{\mathrm{s}})$ and $E^{\mathrm{s}}(I^{\mathrm{s}}-2)$, or γ rays of $E_\gamma^{\mathrm{s}}(I^{\mathrm{s}} \rightarrow I^{\mathrm{s}}-2)$ and $E_\gamma^{\mathrm{s}}(I^{\mathrm{s}}-2 \rightarrow I^{\mathrm{s}}-4)$. As discussed below, such an extended E-GOS curve actually improves the data description.

3 Results and discussion

Table 1 shows our calculated ground-state quadruple β_2, together with the theoretical results calculated by the Hartree-Fock-BCS (HFBCS) [26] and the extended Thomas-Fermi plus Strutinsky integral (ETFSI) methods [27]. Our present equilibrium deformations are obtained within the macroscopic–microscopic theoretical framework, which allows fast calculation in the selected deformation space. The self-consistent HFBCS method may naturally include the necessary deformation degrees of freedom. The ETFSI method combines the advantages of the TRS and HFBCS calculations. The available experimental data are obtained from the reduced transition probabilities $B(E2)$ [28]. One can see that all these three kinds of theoretical results and the experimental values indicate the well-deformed properties of these nuclei. In comparison, the present work based on one-body WS potential gives somewhat small β_2 deformations. Such a difference was observed and analyzed by Dudek et al. [29] 30 years ago according to the relationship between the potential parameters and the nucleonic density distributions, giving the corrected formula, e.g., for protons, $\beta_2^{\rho} \simeq 1.10\beta_2 - 0.03(\beta_2)^3$.

In addition, as an empirical parameter that reflects the shape–phase transition in nuclei, the P factor defined by $P \equiv \frac{N_p N_n}{N_p + N_n}$ is usually helpful to identify nuclear properties [33]. N_p is the minimum number of valence protons or proton holes, and N_n is the corresponding value for neutrons. The product $N_p N_n$ indicates the number of p–n residual interactions, which tend to destroy the spherical symmetry, and the summation $N_p + N_n$ denotes the number of pairing interactions. Near the shell closures, the P factor is very small due to the scarce valence nucleons, and the nucleus presents a spherical shape. Nevertheless, moving away from the closed shells, the increasing valence nucleons will result in an increase in P factor. Obviously, the numerator usually increases faster than the denominator. For instance, in the Yb isotopic chain, the numerator may increase six or more times faster than the denominator, corresponding to 12 proton holes (the difference between the magic number 82 and $Z = 70$). After a critical point, the spherical symmetry of the nucleus will be broken up. In this mass region, the study by Casten et al. [31] indicates that the critical point of the P factor for the transition to deformed shape is about 4–5. As seen in Table 1, the P factors of these nuclei are obviously larger than the critical value, clearly indicating the appearance of large collectivity.

Table 1 The calculated results (TRS) for ground-state equilibrium deformation parameters β_2 in even–even $^{164-178}$Yb, together with the HFBCS [26] and ETFSI [27] calculations and available experimental values (Exp.) [28] for comparison. At the same time, two available empirical quantities, the P factor [30–34] and $R_{4/2}$ [25, 35] are also given for evaluating nuclear collectivity

Nuclei	β_2				P	$R_{4/2}$
	TRS[a]	HFBCS	ETFSI	Expt.[b]		
^{164}Yb	0.249	0.27	0.29	0.291	6.00	3.12
^{166}Yb	0.271	0.28	0.31	0.323	6.46	3.26
^{168}Yb	0.286	0.28	0.31	0.323	6.85	3.26
^{170}Yb	0.293	0.28	0.33	0.326	7.20	3.29
^{172}Yb	0.292	0.32	0.32	0.330	7.50	3.30
^{174}Yb	0.286	0.31	0.33	0.325	7.76	3.30
^{176}Yb	0.278	0.29	0.31	0.306	7.50	3.31
^{178}Yb	0.272	0.28	0.31	–	7.20	3.30

[a]The calculated ground-state $|\gamma|$ values are always less than 1°

[b]The uncertainties are less than 0.01, see Ref. [28]

In the study of low-lying nuclear structure, the energy ratio $R_{4/2} = E_{4_1^+}/E_{2_1^+}$ in even–even nuclei usually can provide a test of the axial assumption. For example, $R_{4/2}$ is 3.3 for a well-deformed axially symmetric rotor, 2.5 for a γ-unstable vibrator, and 2.0 for a spherical vibrator, which, respectively, correspond to $SU(3)$, $O(6)$, and $U(5)$ dynamic symmetries in the algebraic view of the interacting boson model (IBM) [25, 36]. In this table, one notices that all the $R_{4/2}$ values are more than the shape transition point of 3.0 (to quadrupole deformed nuclei) in the Mallmann plot [25]. All these facts support our present calculations to a large extent.

In principle, it is convenient to investigate the yrast state rotational properties in such well-deformed nuclei. The kinematic moment of inertia is generally used to understand the high-spin behaviors of the yrast band in the nucleus. Figure 1 shows the calculated and experimental kinematic moments of inertia obtained using the respective formulas of $J^{(1)} = I_x/\omega$ and $J^{(1)} = \hbar^2(2I - 1)/E_\gamma(I \to I - 2)$. The general trends are in good agreement between theory and experiment. The backbending phenomena are well reproduced by the present calculations, especially in $^{164-170}$Yb. Even the second backbending in the experiment data for ^{168}Yb is replicated by our calculation. However, in $^{172-174}$Yb nuclei, the calculated backbending phenomena are not observed near the expected rotational frequencies. It will be of interest to reveal the mechanism behind this discrepancy and/or further confirm the data in experiments (the intensities of the last several γ rays are weak). In ^{176}Yb, the first upbending phenomenon from the data can be reproduced by the present calculation. In ^{178}Yb, the available data are also in good agreement with theoretical calculations, and the high-spin information is unknown so far.

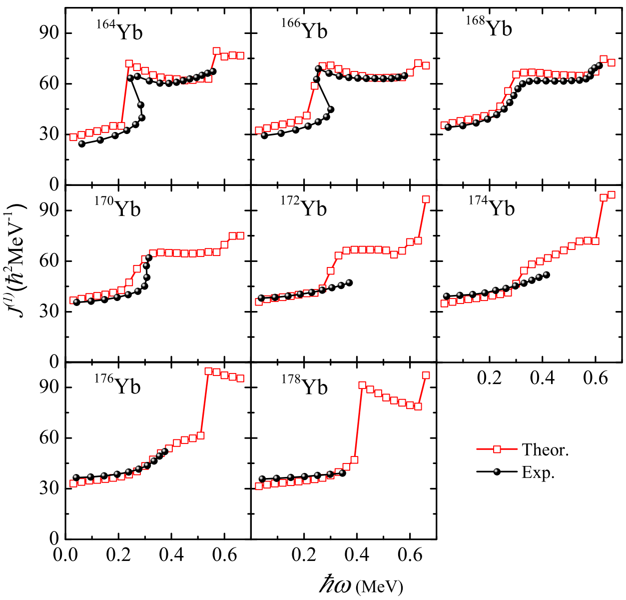

Fig. 1 (Color online) The experimental (filled circle symbols) and calculated (open square symbols) kinematic moments of inertia $J^{(1)}$for even–even nuclei $^{164-178}$Yb as a function of the rotational frequency $\hbar\omega$. The experimental data are taken from Ref [37–42]

To understand the behaviors displayed by the moments of inertia, in Fig. 2, we present the proton, neutron, and total aligned angular momenta. From Fig. 2, the rotation alignments of proton and/or neutron pairs near the Fermi surface can be evaluated. Such a band crossing between 0 quasi-particle and 2 quasi-particle bands can usually be used to explain the observed backbending or upbending phenomena. It can be seen clearly that in these nuclei the first backbending or upbending phenomenon originates from the neutron alignments (here, the candidates of the related high-j orbits are $2f_{7/2}$, $1h_{9/2}$, and $1i_{13/2}$). With increasing neutron number, the backbending phenomena evolve into upbending due to the increasing interaction between the 0 quasi-particle and 2 quasi-particle bands. Simultaneously, the backbending/upbending frequencies are delayed with the increasing neutron number. In particular, the simultaneous alignments for neutron and proton pairs appear, which awaits to be identified in experiment in the future. Actually, such competition phenomena have been discussed in other mass regions [43, 44]. It is worth noting that a shape jump may sometimes be responsible for the large alignment, instead of the simultaneous decoupling of proton and neutron pairs [45]. For instance, shape transition from prolate to oblate occurs at $\hbar\omega \approx 0.4$ MeV in ^{178}Yb, cf. Fig. 4. In addition, the proton $h_{11/2}$ alignment was used to explain the second band crossing of ^{168}Yb (in which the high-spin states up to $I = 38$ have been observed experimentally) by Fitzpatrick et al. [39], in good agreement with our calculations.

Figures 3 and 4 show the deformation Routhian curves as function of β_2 and γ deformation degrees of freedom, respectively. Of course, we would like to point out that the Bohr shape deformation parameters [46] are adopted here. The quadrupole deformation β_2 is always nonnegative. The prolate, oblate, and triaxial shapes are denoted by the γ deformation parameter, e.g., from $0° < \gamma < 60°$. In this

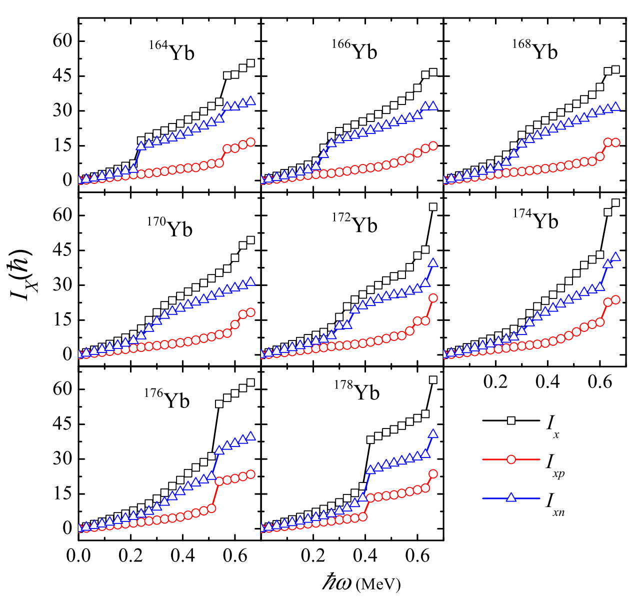

Fig. 2 (Color online) The calculated aligned angular momenta I_x (squares), including the proton I_{xp} (circles) and neutron I_{xn} (triangles) components, for even–even nuclei $^{164-178}$Yb as a function of the rotational frequency

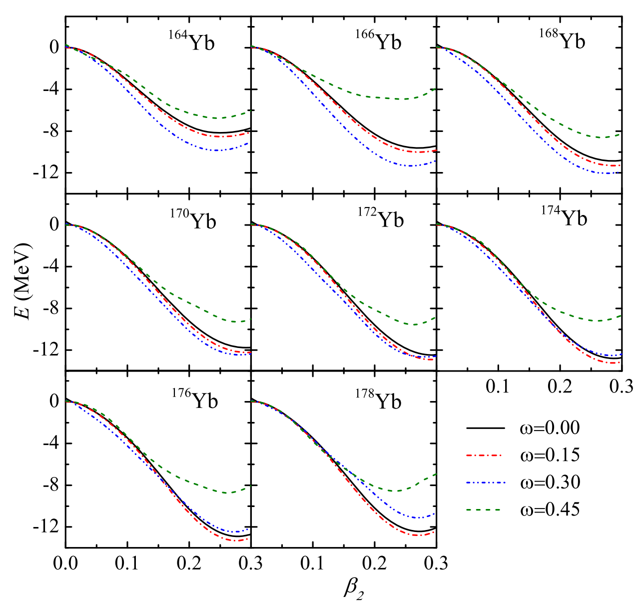

Fig. 3 (Color online) Deformation Routhian curves (normalized to the energies at $\beta_2 = 0.0$) against β_2 for even–even $^{164-178}$Yb nuclei at several selected rotational frequencies: ω = 0.00 (black), 0.15 (red), 0.30 (blue), and 0.45 (green) MeV/$\hbar$. At each β_2 point, the energy has been minimized with respect to γ and β_4

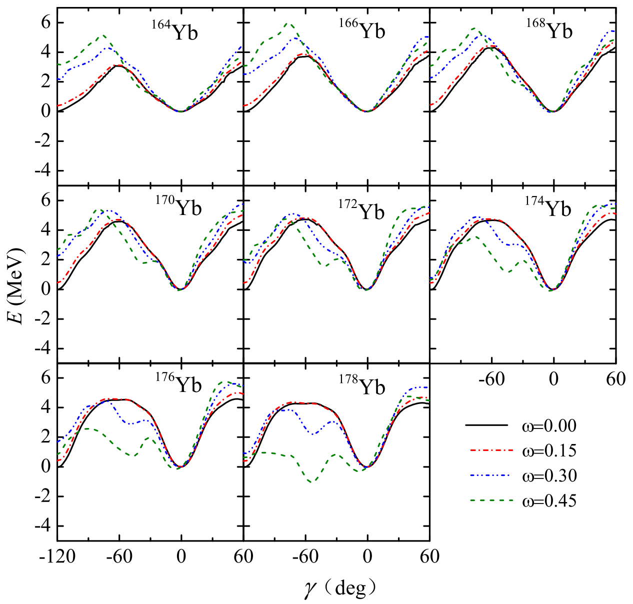

Fig. 4 (Color online) Deformation Routhian curves against γ for even–even $^{164-178}$Yb nuclei at selected rotational frequencies, similar to Fig. 3

work, we adopt the Lund convention [47] with $-120° \leq \gamma \leq 60°$, which is convenient for describing the cranking motion. Such a range is divided into three sectors, $-120° < \gamma < -60°$, $-60° < \gamma < 0°$, and $0° < \gamma < 60°$, representing rotation regarding the long, intermediate, and short axes, respectively. The critical values 0° ($-120°$) and $-60°$ (60°) correspond to axially symmetric shapes (prolate and oblate, respectively). Further, $\gamma = -120°$ and 60° mean the nucleus rotates around its symmetry axis. In other words, non-collective rotation and $\gamma = -60°$ or 0° will mean the nucleus rotates around an axis perpendicular to its symmetry axis (that is, collective rotation).

Based on these curves, the shape stabilities and nuclear stiffness under rotation can be analyzed, which are model-independent to some extent [48]. Note that we are only concerned about the deformation Routhian curves near the minima, which are somewhat symmetric. Therefore, according to the equilibrium deformation values shown in Table 1, the energy curves from $\beta_2 = 0.0$ to 0.3 are plotted, as this is sufficient to understand the stiffness properties. When moving away from the $N = 104$ midshell nucleus ^{174}Yb, it seems that the nuclei become gradually softer at the ground states as expected. For each nucleus, the equilibrium β_2 and nuclear stiffness may slightly increase at low spins relative to that at the ground state. Whereas, at high rotational frequency the curve becomes flat, indicating the appearance of high softness. In the triaxial direction, as shown in Fig. 4, the γ deformations in $^{164-170}$Yb are stable within the present rotational frequency range. The later four nuclei $^{172-178}$Yb are unstable in the γ direction. In particular, in ^{178}Yb nucleus, the oblate shape clearly occurs at $\hbar\omega = 0.45$ MeV.

The deformation Routhian curves indicate that the shape/phase or nuclear stiffness may change with rotation. Naturally, it will be interesting to investigate the shape/phase transition and possible vibrational effects due to the large softness. The existing difference in moments of inertia between theory and experiment may also be explained to an extent. The model adopted here does not include the vibrational mechanism, although it can well describe the rotational properties of nuclei. Fortunately, an empirical method, called the E-GOS (E-gamma over spin) curves [namely, the simple function $R(I) = E_\gamma(I \to I - 2)/I$], was proposed by Regan et al. [11], which can manifest the shape/phase transition between vibration and rotation along the yrast line. To better describe the evolution of the modes of motion, we recently extended such empirical curves to the centipede-like ones including γ-soft mode [12, 13]. Figure 5 displays the centipede-like E-GOS curves for even–even $^{164-178}$Yb isotopes. Indeed, one can see that the signature of transition from rotation to γ-soft or from vibration to rotation appears in $^{164-168}$Yb, as mentioned by Shen et al. [49]. Similar transitions seem to take place in other nuclei, although they still need to be experimentally confirmed because of the scarcity of data. It should be noted that three idealized assumptions (e.g., rotation, γ-soft, and vibration) are adopted when plotting the centipede-like E-GOS curves.

Obviously, if there is coupling between different motion modes, the assumption of the purely single-mode motion will be somewhat unreasonable. To empirically test

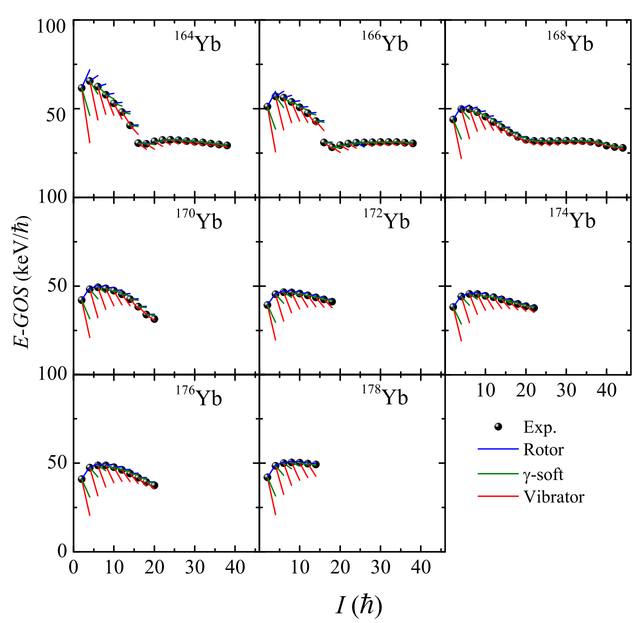

Fig. 5 (Color online) The centipede-like E-GOS curves along the yrast sequences for even–even $^{164-178}$Yb isotopes

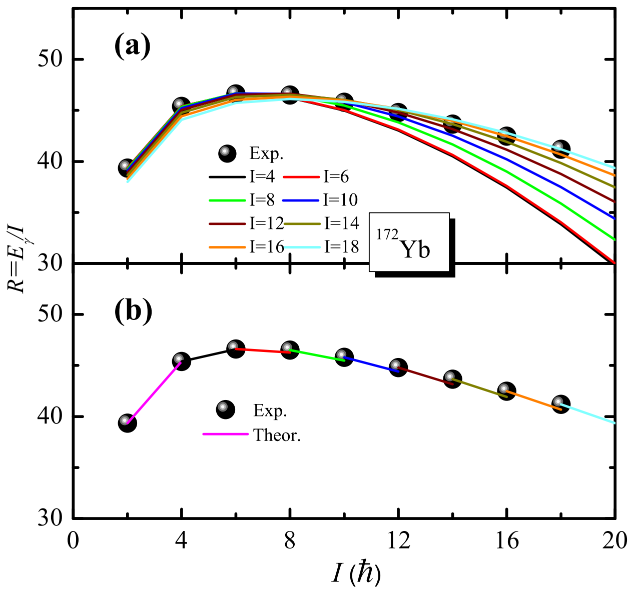

Fig. 6 (Color online) **a** The E-GOS curves after including the first-order rotation–vibration interaction [25] for ^{172}Yb. The curve with different colors indicates that it crosses the corresponding $R(I)$ data. **b** The improved E-GOS curve constituted by the $R(I) \rightarrow R(I+2)$ line segments

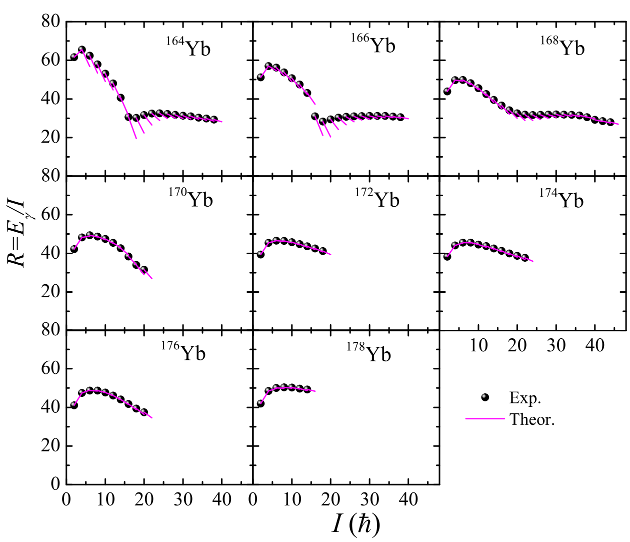

Fig. 7 (Color online) Improved E-GOS curves along the yrast sequences for even–even $^{164-178}$Yb isotopes, similar to Fig. 6b

whether the coupling effect will play a role under rotation, we further improve the E-GOS curve as introduced in Sect. 2. According to the energy expression given by Mallmann [25], taking the rotation–vibration interaction into account, we can plot a set of E-GOS curves based on the derived function relation $R(I)$ and the adjacent levels or the γ rays. It is reasonable to assume that adjacent points have the similar motion modes, except for the critical point of shape/phase transition. In Fig. 6a as an example, for the nucleus ^{172}Yb none of the curves could pass through all the data points, showing somewhat large changes in the coefficients (e.g., a and b) in Eq. (1) when the data points are far from each other. However, it turned out that the third data point determined by the two preceding data points will fall on the $R(I)$ curve. Similar to our previous work, an improved E-GOS "curve" can be obtained by retaining the $R(I^s) \rightarrow R(I^s+2)$ line segments for each E-GOS curve, as shown in Fig. 6b. Thus, one can say that the rotation–vibration coupling will evidently play a role, but the coupling coefficients may change with rotation. Figure 7 shows our improved E-GOS curves for $^{164-178}$Yb nuclei in the present work. Compared with Fig. 5, it is found that such an improvement in the E-GOS curve may explain and predict the data better. The large deviation in Fig. 7 originates from the irregular E_γ values due to the band crossings. In the letter by Mallmann, it has been noted that when the energy ratio $R_{4/2} \gtrsim 2.67$, the energy formula in Eq. (1) is valid. As seen in Table 1, the smallest $R_{4/2}$ value in $^{164-178}$Yb is obviously greater than this value. The new E-GOS curve indicates that the vibration effect may be somewhat important even in these well-deformed nuclei. Further tests should be conducted in this regard. If so, the inclusion of such a vibration mechanism in the theoretical model will be considered in our future work.

4 Summary

We have systematically investigated the collective properties along the yrast line for well-deformed even–even $^{164-178}$Yb nuclei, based on the pairing-deformation self-consistent TRS method in the $(\beta_2, \gamma, \beta_4)$ deformation space. As a basic test, the calculated equilibrium deformations at ground states and the backbending behavior in the moment of inertia are compared with previous theoretical and/or experimental data and show good agreement. It is found that the backbending behavior in the moment of inertia can generally be satisfactorily explained by the alignment of a pair of nucleons. The band crossing between prolate and oblate ones may be misunderstood by the physical picture of proton and neutron simultaneous decoupling, i.e., in ^{178}Yb (which awaits experimental confirmation). Based on the corresponding deformation energy/Routhian curves, we also evaluate the evolution of nuclear stiffness in both the β_2 and γ directions. In addition, the evolution among different collective modes along the yrast line is investigated on the basis of the centipede-like E-GOS curves, which partly explain the existing differences in the moment of inertia between theory and experiment. Taking the coupling of rotational and vibrational motions into account, the present work further extended the

E-GOS curve to better describe the evolution trend in the data. Therefore, models including the rotation–vibration coupling may be interesting and meaningful in future work.

References

1. R. Lucas, Nuclear shapes. Europhys. News **32**, 5 (2001). https://doi.org/10.1051/epn:2001101
2. Nationl Nuclear Data Center. http://www.nndc.bnl.gov/. Accessed 20 Oct 2017
3. W. Ogle, S. Wahlborn, R. Piepenbring et al., Single-particle levels of nonspherical nuclei in the region $150 < A < 190$. Rev. Mod. Phys. **43**, 424 (1971). https://doi.org/10.1103/RevModPhys.43.424
4. S. Wahlborn, Effects of blocking on the level spacings of odd-mass deformed nuclei. Nucl. Phys. **37**, 554 (1962). https://doi.org/10.1016/0029-5582(62)90290-0
5. G. Ehrling, S. Wahlborn, Single-particle model calculations for deformed nuclei of spheroidal and non-spheroidal shapes. Phys. Scripta **6**, 94 (1972). https://doi.org/10.1088/0031-8949/6/2-3/002
6. W. Satuła, R. Wyss, P. Magierski et al., The Lipkin–Nogami formalism for the cranked mean field. Nucl. Phys. A **578**, 45 (1994). https://doi.org/10.1016/0375-9474(94)90968-7
7. F.R. Xu, W. Satuła, R. Wyss, Quadrupole pairing interaction and signature inversion. Nucl. Phys. A **669**, 119 (2000). https://doi.org/10.1016/S0375-9474(99)00817-9
8. Z.H. Zhang, X.T. He, J.Y. Zeng et al., Systematic investigation of the rotational bands in nuclei with $Z \approx 100$ using a particle-number conserving method based on a cranked shell model. Phys. Rev. C **85**, 014324 (2012). https://doi.org/10.1103/PhysRevC.85.014324
9. K. Hara, Y. Sun, Projected shell model and high-spin spectroscopy. Int. J. Mod. Phys. E **4**, 637 (1995). https://doi.org/10.1142/S0218301395000250
10. Z. Shi, Z.H. Zhang, Q.B. Chen et al., Shell-model-like approach based on cranking covariant density functional theory: band crossing and shape evolution in ^{60}Fe. Phys. Rev. C **97**, 034317 (2018). https://doi.org/10.1103/PhysRevC.97.034317
11. P.H. Regan, C.W. Beausang, N.V. Zamfir et al., Signature for vibrational to rotational evolution along the yrast line. Phys. Rev. Lett. **90**, 152502 (2003). https://doi.org/10.1103/PhysRevLett.90.152502
12. Q. Yang, H.L. Wang, M.L. Liu et al., Characteristics of collectivity along the yrast line in even–even tungsten isotopes. Phys. Rev. C **94**, 024310 (2016). https://doi.org/10.1103/PhysRevC.94.024310
13. J. Yang, H.L. Wang, Q.Z. Chai et al., Evolution of shape and rotational structure in neutron-deficient $^{118-128}$Ba nuclei. Prog. Theor. Exp. Phys. **2016**, 063D03 (2016). https://doi.org/10.1093/ptep/ptw074
14. H.Y. Meng, H.L. Wang, Q.Z. Chai et al., Possible properties on nuclear shape and stiffness evolution: a systematic analysis based on nuclear-energy-surface calculations. Nucl. Phys. Rev. **34**, 481 (2017). https://doi.org/10.11804/NuclPhysRev.34.03.481
15. Q.Z. Chai, W.J. Zhao, H.L. Wang et al., Possible observation of shape-coexisting configurations in even-even midshell isotones with $N = 104$: a systematic total Routhian surface calculation. Nucl. Sci. Tech. **29**, 38 (2018). https://doi.org/10.1007/s41365-018-0381-5
16. W. Nazarewicz, G.A. Leander, J. Dudek, Octupole shapes and shape changes at high spins in Ra and Th nuclei. Nucl. Phys. A **467**, 437 (1987). https://doi.org/10.1016/0375-9474(87)90539-2
17. R. Bengtsson, S. Frauendorf, Quasiparticle spectra near the yrast line. Nucl. Phys. A **327**, 139 (1979). https://doi.org/10.1016/0375-9474(79)90322-1
18. S. Frauendorf, Spin alignment in heavy nuclei. Phys. Scripta **24**, 349 (1981). https://doi.org/10.1088/0031-8949/24/1B/034
19. W.D. Myers, W.J. Swiatecki, Nuclear masses and deformations. Nucl. Phys. **81**, 1 (1966). https://doi.org/10.1016/0029-5582(66)90639-0
20. V.M. Strutinsky, Shell effects in nuclear masses and deformation energies. Nucl. Phys. A **95**, 420 (1967). https://doi.org/10.1016/0375-9474(67)90510-6
21. H.C. Pradhan, Y. Nogami, J. Law, Study of approximations in the nuclear pairing-force problem. Nucl. Phys. A **201**, 357 (1973). https://doi.org/10.1016/0375-9474(73)90071-7
22. P. Möller, J.R. Nix, Nuclear pairing models. Nucl. Phys. A **536**, 20 (1992). https://doi.org/10.1016/0375-9474(92)90244-E
23. H. Sakamoto, T. Kishimoto, Origin of the multipole pairing interactions. Phys. Lett. B **245**, 321 (1990). https://doi.org/10.1016/0370-2693(90)90651-L
24. Q.Z. Chai, W.J. Zhao, M.L. Liu et al., Calculation of multidimensional potential energy surfaces for even-even transuranium nuclei: systematic investigation of the triaxiality effect on the fission barrier. Chin. Phys. C **42**, 5 (2018). https://doi.org/10.1088/1674-1137/42/5/054101
25. C.A. Mallmann, System of levels in even-even nuclei. Phys. Rev. Lett. **2**, 507 (1959). https://doi.org/10.1103/PhysRevLett.2.507
26. S. Goriely, F. Tondeur, J.M. Pearson, A Hartree–Fock nuclear mass table. At. Data Nucl. Data Tables **77**, 311 (2001). https://doi.org/10.1006/adnd.2000.0857
27. Y. Aboussir, J.M. Pearson, A.K. Dutta et al., Nuclear mass formula via an approximation to the Hartree–Fock method. At. Data Nucl. Data Tables **61**, 127 (1995). https://doi.org/10.1016/S0092-640X(95)90014-4
28. S. Raman, C.W. Nestorjr, P. Tikkaned, Transition probability from the ground to the first-excited 2^+ state of even-even nuclides. At. Data Nucl. Data Tables **78**, 1 (2001). https://doi.org/10.1006/adnd.2001.0858
29. J. Dudek, W. Nazarewicz, P. Olanders, On the shape consistency in the deformed shell-model approach. Nucl. Phys. A **420**, 285 (1984). https://doi.org/10.1016/0375-9474(84)90443-3
30. N. Fouladi, J. Fouladi, H. Sabri, Investigation of low-lying energy spectra for deformed prolate nuclei via partial dynamical SU(3) symmetry. Eur. Phys. J. Plus **130**, 112 (2015). https://doi.org/10.1140/epjp/i2015-15112-7
31. R.F. Casten, D.S. Brenner, P.E. Haustein, Valence *p-n* interactions and the development of collectivity in heavy nuclei. Phys. Rev. Lett. **58**, 658 (1987). https://doi.org/10.1103/PhysRevLett.58.658
32. R.F. Casten, Possible unified interpretation of heavy nuclei. Phys. Rev. Lett. **54**, 1991 (1985). https://doi.org/10.1103/PhysRevLett.54.1991
33. R.F. Casten, N_pN_n systematics in heavy nuclei. Nucl. Phys. A **443**, 1 (1985). https://doi.org/10.1016/0375-9474(85)90318-5
34. R.F. Casten, N.V. Zamfir, The evolution of nuclear structure: the N_pN_n scheme and related correlations. J. Phys. G: Nucl. Part. Phys. **22**, 1521 (1996). https://doi.org/10.1088/0954-3899/22/11/002
35. M.A.J. Mariscotti, Rotational description of states in closed-and near-closed-shell nuclei. Phys. Rev. Lett. **24**, 1242 (1970). https://doi.org/10.1103/PhysRevLett.24.1242
36. J.B. Gupta, New perspective in rotation–vibration interaction. Int. J. Mod. Phys. E **22**, 1350023 (2013). https://doi.org/10.1142/S0218301313500237

37. A. Nordlund, R. Bengtsson, P. Ekströmp et al., Probing the limits of complete spectroscopy in ^{164}Yb. Nucl. Phys. A **591**, 117 (1995). https://doi.org/10.1016/0375-9474(95)00124-J
38. C.A. Fields, K.H. Hicks, R.J. Peterson, Band crossings at low rotational frequency in ^{166}Yb. Nucl. Phys. A **431**, 473 (1995). https://doi.org/10.1016/0375-9474(84)90119-2
39. A. Fitzpatrick, S.Y. Araddad et al., Proton alignments at high rotational frequency in ^{167,168}Yb. Nucl. Phys. A **582**, 335 (1995). https://doi.org/10.1016/0375-9474(94)00459-Z
40. P.M. Walker, S.R. Faber, W.H. Bentley et al., Negative-parity yrast band in ^{170}Yb: rotation-aligned neutrons with deformation-coupled bandhead? Phys. Lett. B **81**, 9 (1979). https://doi.org/10.1016/0370-2693(79)90608-7
41. S.J. Asztalos, I.Y. Lee, K. Vetter et al., Spin yields of neutron-rich nuclei from deep inelastic reactions. Phys. Rev. C **60**, 044307 (1999). https://doi.org/10.1103/PhysRevC.60.044307
42. I.Y. Lee, S. Asztalos, M.A. Deleplanque et al., Study of neutron-rich nuclei using deep-inelastic reactions. Phys. Rev. C **56**, 753 (1997). https://doi.org/10.1103/PhysRevC.56.753
43. H.L. Wang, Q.Z. Chai, J.G. Jiang et al., Rotational properties in even-even superheavy $^{254-258}$Rf nuclei based on total-Routhian-surface calculations. Chin. Phys. C **38**, 7 (2014). https://doi.org/10.1088/1674-1137/38/7/074101
44. F. Al-khudair, G.L. Long, Y. Sun, Competition in rotation-alignment between high-*j* neutrons and protons in transfermium nuclei. Phys. Rev. C **79**, 034320 (2009). https://doi.org/10.1103/PhysRevC.79.034320
45. P.M. Walker, P.O. Arve, J. Simpson et al., Double crossing in ^{174}Hf: A deformation jump? Phys. Lett. B **168**, 326 (1986). https://doi.org/10.1016/0370-2693(86)91638-2
46. A. Bohr, Quadrupole degree of freedom for the nuclear shape. Mat. Fys. Medd. K. Dan. Vidensk. Selsk. **26**, 1 (1952)
47. G. Andersson, S.E. Larsson, G. Leander et al., Nuclear shell structure at very high angular momentum. Nucl. Phys. A **268**, 205 (1976). https://doi.org/10.1016/0375-9474(76)90461-9
48. H.L. Wang, J. Yang, M.L. Liu et al., Evolution of ground-state quadrupole and octupole stiffnesses in even–even barium isotopes. Phys. Rev. C **92**, 024303 (2015). https://doi.org/10.1103/PhysRevC.92.024303
49. S.F. Shen, Y.B. Chen, F.R. Xu et al., Signature for rotational to vibrational evolution along the yrast line. Phys. Rev. C **75**, 047304 (2007). https://doi.org/10.1103/PhysRevC.75.047304